

Local gravitational instability of two-component thick discs in three dimensions

Carlo Nipoti¹, Cristina Caprioglio¹ and Cecilia Bacchini²

¹ Dipartimento di Fisica e Astronomia “Augusto Righi”, Università di Bologna, via Gobetti 93/2, 40129, Bologna, Italy
e-mail: carlo.nipoti@unibo.it

² DARK, Niels Bohr Institute, University of Copenhagen, Jagtvej 155, 2200 Copenhagen, Denmark

Accepted, May 20, 2024

ABSTRACT

Aims. The local gravitational instability of rotating discs is believed to be an important mechanism in different astrophysical processes, including the formation of gas and stellar clumps in galaxies. We aim to study in three dimensions the local gravitational instability of two-component thick discs.

Methods. We take as starting point a recently proposed analytic three-dimensional (3D) instability criterion for discs with non-negligible thickness which takes the form $Q_{3D} < 1$, where Q_{3D} is a 3D version of the classical 2D Toomre Q parameter for razor-thin discs. Here we extend the 3D stability analysis to two-component discs, considering first the influence on Q_{3D} of a second unresponsive component, and then the case in which both components are responsive. We present the application to two-component discs with isothermal vertical distributions, which can represent, for instance, galactic discs with both stellar and gaseous components. Finally, we relax the assumption of vertical isothermal distribution, by studying one-component self-gravitating discs with polytropic vertical distributions for a range of values of the polytropic index corresponding to convectively stable configurations.

Results. We find that $Q_{3D} < 1$, where Q_{3D} can be computed from observationally inferred quantities, is a robust indicator of local gravitational instability, depending only weakly on the presence of a second component and on the vertical gradient of temperature or velocity dispersion. We derive a sufficient condition for local gravitational instability in the midplane of two-component discs, which can be employed when both components have $Q_{3D} > 1$.

Key words. galaxies: kinematics and dynamics – galaxies: star formation – instabilities – planets and satellites: formation – protoplanetary discs – stars: formation

1. Introduction

The local gravitational instability of rotating fluids is an important phenomenon in several astrophysical systems, ranging from protoplanetary discs to galactic discs. In the case of razor-thin rotating discs, Toomre (1964) derived an analytic instability criterion against small axisymmetric perturbations. However, observations of astrophysical systems showed that the assumption of infinitesimally thin discs is often not realistic. For instance, both gaseous and stellar discs in nearby star-forming galaxies have non-negligible thickness of $\sim 0.1 - 1$ kpc (e.g. O’Brien et al. 2010; van der Kruit & Freeman 2011; Yim et al. 2014; Mackereth et al. 2017; Marchuk & Sotnikova 2017). Different modifications to 2D Toomre’s analysis that approximately account for the finite thickness of the disc have been proposed in several works (e.g. Toomre 1964; Vandervoort 1970; Romeo 1992; Bertin & Amorisco 2010; Wang et al. 2010; Elmegreen 2011; Griv & Gedalin 2012; Romeo & Falstad 2013; Behrendt et al. 2015).

In many cases, astrophysical discs are not purely self-gravitating, but belong to multi-component systems. A typical case is that of late-type galaxies, in which gaseous discs coexist with stellar discs and with pressure supported components like bulges and dark-matter halos. When two or more discs coexist, the local gravitational stability of each disc can be influenced by the interplay with the other disc, because any gravitational per-

turbation affect both discs at the same time (Toomre 1964). The stability of multi-component discs has been widely studied in the literature in the case of infinitesimally thin discs and also in 2D analyses that account approximately for the finite disc thickness (Lin & Shu 1966; Kato 1972; Jog & Solomon 1984a,b; Romeo 1994; Wang & Silk 1994; Elmegreen 1995; Rafikov 2001; Shen & Lou 2003; Romeo & Wiegert 2011).

Nipoti (2023, hereafter N23) presented a three-dimensional (3D) stability analysis of rotating stratified fluids, which generalizes previous 3D studies that obtained instability criteria based on more restrictive assumptions (Safronov 1960; Chandrasekhar 1961; Goldreich & Lynden-Bell 1965a,b; Genkin & Safronov 1975; Bertin & Casertano 1982; Mamatsashvili & Rice 2010; Meidt 2022). Here we extend the work of N23, by studying in 3D the local gravitational instability of two-component discs. We first consider the influence on the 3D instability parameter of a second unresponsive component, and then the case in which both components are responsive. We present the application to two-component discs with isothermal vertical distributions, which can represent, for instance, galactic discs with both stellar and gaseous components. Finally, we relax the assumption of vertical isothermal distribution, by studying self-gravitating discs with vertical polytropic distribution, and thus in general with non-zero vertical temperature or velocity-dispersion gradients. Though the computation of two-component discs with generic polytropic vertical distributions is not more technically difficult

than that of two-component isothermal discs, in this work we present results on the polytropic case only for one-component discs, which is a clean case study that allows us to quantify the effect of non-isothermality, without exploring the larger parameter space of two-component systems.

The paper is organized as follows. Section 2 recalls some relevant equations of previous disc stability analyses. In section 3 we describe the properties of two-component disc models with vertical isothermal distributions. The question of the linear stability in 3D of two-component discs with both components responsive is addressed Section 4. Disc with vertical polytropic distributions are discussed in Section 5 and Section 6 concludes.

2. Preliminaries

In this work we study axisymmetric rotating fluid disc models, adopting, as it is natural, a cylindrical system of coordinates (R, z, ϕ) . As we limit our stability analysis to axisymmetric perturbations, none of the quantities considered in this paper depends on ϕ . Let us consider the properties of a disc at given radius R . The disc surface density is

$$\Sigma = \int_{-\infty}^{\infty} \rho(z) dz, \quad (1)$$

where $\rho(z)$ is vertical volume density profile. We assume that $\rho(z)$ is such that Σ is finite, and we introduce as a reference vertical scale the half-mass half-height z_{half} , defined to be such that

$$\frac{1}{\Sigma} \int_{-z_{\text{half}}}^{z_{\text{half}}} \rho(z) dz = 0.5. \quad (2)$$

The classical Toomre (1964) 2D criterion for gravitational instability of razor-thin rotating discs is $Q < 1$, where

$$Q \equiv \frac{\kappa \sigma}{\pi G \Sigma} \quad (3)$$

is Toomre's instability parameter at a given radius. Here κ is the epicyclic frequency, defined by

$$\kappa^2 \equiv 4\Omega^2 + \frac{d\Omega^2}{d \ln R}, \quad (4)$$

with Ω is the angular frequency, assumed throughout this paper to depend only on R , and σ is the gas velocity dispersion defined by $\sigma^2 \equiv P/\rho$. The quantity σ can be interpreted also as the *isothermal* sound speed of the fluid, but we prefer to refer to σ generically as the velocity dispersion, because this allows us to have more flexibility in the physical interpretation of the fluid, which can represent not only a standard smooth gas supported by thermal pressure, but also a turbulent gas, a gas composed of discrete gas clouds or even a stellar distribution (see Section 3.2).

2.1. The 3D gravitational instability criterion

We take as starting point the results of N23, who studied in 3D the local gravitational instability of rotating stratified fluids. Among the configurations considered by N23, we consider the simplest: vertically stratified discs (section 3.3 of N23), in which it is assumed $\Omega = \Omega(R)$ and that the radial gradients of pressure and density are locally negligible. N23 has shown that a sufficient condition for local gravitational instability at given (R, z) in such a vertically stratified disc is

$$Q_{3D} \equiv \frac{\sqrt{k^2 + \nu^2} + c_s h_z^{-1}}{\sqrt{4\pi G \rho}} < 1 \quad (\text{sufficient for instability}),$$

(5)

where ν , defined by

$$\nu^2 \equiv \frac{\rho'_z p'_z}{\rho^2} = \frac{c_s^2}{\gamma} \frac{\rho'_z}{\rho} \frac{p'_z}{p}, \quad (6)$$

is a frequency related to vertical pressure and density gradients ($\rho'_z \equiv \partial \rho / \partial z$, $p'_z \equiv \partial p / \partial z$), h_z is a measure of the disc thickness, and $c_s = \sqrt{\gamma} \sigma$ is the sound speed¹, with $\gamma \equiv (\rho/p) dp/d\rho$, in which dp is the pressure variation corresponding to a density variation $d\rho$ during a transformation. Following N23, throughout the paper we assume $h_z = h_{70\%}$, where $h_{70\%}$, defined by

$$\frac{1}{\Sigma} \int_{-h_{70\%/2}}^{h_{70\%/2}} \rho(z) dz = 0.7, \quad (7)$$

is the height of an infinitesimal-width strip centred on the midplane containing 70% of the mass per unit surface. The scale height h_z appearing in the definition of Q_{3D} derives from the approximation used by N23 for the linearized Poisson equation for radial perturbations. In Appendix A we assess quantitatively the validity of this approximation when $h_z = h_{70\%}$, by considering one-component discs. In the following we will adopt $h_z = h_{70\%}$ also for two-component discs, assuming that it remains a sufficiently good approximation also in the presence of a second component.

2.2. Discs with self-gravitating isothermal vertical distribution

Before discussing more generic models, it is useful to recall the properties of a disc in which the vertical density distribution is that of the self-gravitating isothermal (SGI) slab (Spitzer 1942)

$$\rho(z) = \rho_0 \operatorname{sech}^2 \tilde{z}, \quad (8)$$

where $\rho_0 = \rho(0)$ is the density in the midplane and $\tilde{z} \equiv z/b$, with $b \equiv \sigma / \sqrt{2\pi G \rho_0}$ a scale height, where σ is the z -independent velocity dispersion. The gravitational potential is

$$\Phi(z) = -\sigma^2 \ln \left[\frac{\rho(z)}{\rho_0} \right] \quad (9)$$

and the surface density is $\Sigma = 2b\rho_0$, so $\rho_0 = \pi G \Sigma^2 / (2\sigma^2)$. Using $p(z) = \sigma^2 \rho(z)$, Eq. (6) and Eq. (8), we obtain that for the SGI disc model we have

$$\nu^2 = 8\pi G \rho_0 \tanh^2 \tilde{z}. \quad (10)$$

So, for a disc with angular velocity $\Omega = \Omega(R)$ and SGI vertical distribution, at any given R the sufficient condition for instability (5) becomes (N23)

$$Q_{3D} = \sqrt{\frac{Q^2}{2} \cosh^2 \tilde{z} + 2 \sinh^2 \tilde{z}} + \sqrt{\frac{\gamma}{2}} \frac{b}{h_z} \cosh \tilde{z} < 1 \quad (\text{sufficient for instability}). \quad (11)$$

¹ The sound speed c_s as defined here is in general different from the gas velocity dispersion (or *isothermal* sound speed) σ . For instance, an ideal monoatomic gas that undergoes adiabatic transformations has $\gamma = 5/3$ and $c_s = \sqrt{5/3} \sigma$, while for a fluid that undergoes isothermal transformations $\gamma = 1$ and $c_s = \sigma$. Note that in the adopted notation γ is not necessarily the heat capacity ratio: it is the heat capacity ratio for an ideal gas undergoing adiabatic transformations.

3. Two-component discs with isothermal vertical distributions

We consider here two-component discs, in which each component has an isothermal vertical density distribution.

3.1. Equations

To describe a two-component disc, we use the index i (for $i = 1, 2$) to label the generic i th component. At any given R the vertical equilibrium is described by a two-component isothermal slab (see Bertin & Pegoraro 2022) composed of two components with density distributions $\rho_1(z)$ and $\rho_2(z)$ in equilibrium in the total gravitational potential

$$\Phi(z) = \Phi_1(z) + \Phi_2(z), \quad (12)$$

where Φ_i , satisfying

$$\frac{d^2\Phi_i}{dz^2} = 4\pi G\rho_i, \quad (13)$$

is the gravitational potential generated by ρ_i . Each component is in vertical hydrostatic equilibrium in the total potential Φ , so

$$\frac{dp_i}{dz} = -\rho_i \frac{d\Phi}{dz}, \quad (14)$$

where $p_i(z) = \sigma_i^2 \rho_i(z)$, σ_i and $\rho_i(z)$ are, respectively, the pressure, velocity dispersion and density of the i th component. Given that σ_i is independent of z , Eq. (14) can be written as

$$\sigma_i^2 \frac{d \ln \rho_i}{dz} = -\frac{d\Phi}{dz}, \quad (15)$$

which has solution

$$\rho_i(z) = \rho_{0,i} e^{-\Phi/\sigma_i^2}, \quad (16)$$

where $\rho_{0,i}$ is the midplane density of the i th component.

Combining Eqs. (12), (13) and (16), we get the ordinary differential equation

$$\frac{d^2\Phi}{dz^2} = 4\pi G \left(\rho_{0,1} e^{-\Phi/\sigma_1^2} + \rho_{0,2} e^{-\Phi/\sigma_2^2} \right), \quad (17)$$

which, for given $\rho_{0,1}$, $\rho_{0,2}$, σ_1 and σ_2 , can be solved to obtain $\Phi(z)$, and then $\rho_1(z)$ and $\rho_2(z)$ from Eq. (16). Eq. (17) can be written in dimensionless form as

$$\frac{d^2\tilde{\Phi}}{d\tilde{z}^2} = 2 \left(e^{-\tilde{\Phi}} + \xi e^{-\tilde{\Phi}/\mu} \right), \quad (18)$$

where $\tilde{\Phi} \equiv \Phi/\sigma_1^2$, $\mu \equiv \sigma_2^2/\sigma_1^2$, $\xi \equiv \rho_{0,2}/\rho_{0,1}$ and $\tilde{z} \equiv z/b_1$, with $b_1 \equiv \sigma_1/\sqrt{2\pi G\rho_{0,1}}$ a scale height. The two-component isothermal slab models as defined above have only two free parameters: ξ (the central density ratio of the two components) and μ (their velocity dispersion ratio squared). Assuming that the two components share the same κ , we define the Q parameter of the i th component as

$$Q_i = \frac{\kappa\sigma_i}{\pi G\Sigma_i}, \quad (19)$$

where Σ_i is the surface density of the i th component.

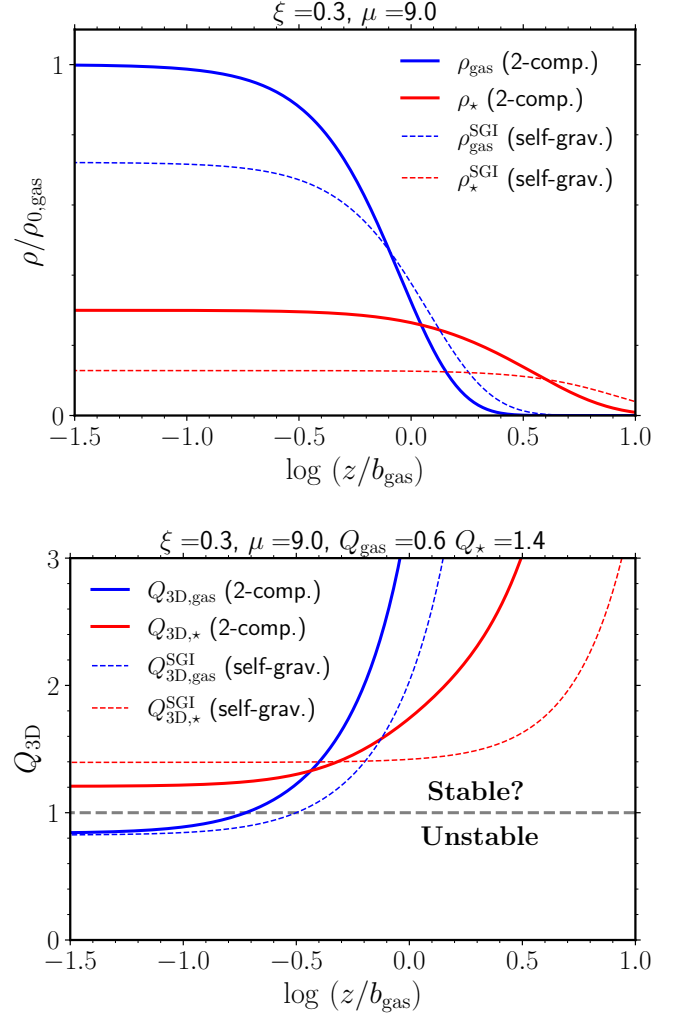


Fig. 1: Upper panel. Vertical density profiles (solid curves) of gas and stars of a two-component isothermal disc with $\mu = 9$ and $\xi = 0.3$. The dashed curves are the profiles of the corresponding SGI models with the same velocity dispersion and surface density. Lower panel. Vertical Q_{3D} profiles of the same models as in the upper panel, assuming $Q_{\text{gas}} = 0.6$ (and thus $Q_{\star} = 1.4$). The horizontal dashed line indicates the instability threshold $Q_{3D} = 1$. Here $\rho_{0,\text{gas}}$ and b_{gas} are, respectively, the midplane density and the scale height of the gaseous component of the two-component disc.

3.2. Vertical density profiles

We present here an example of an equilibrium two-component isothermal model obtained by solving numerically Eq. (18) for given values of the parameters μ and ξ , with boundary conditions $\tilde{\Phi} = 0$ and $d\tilde{\Phi}/d\tilde{z} = 0$ at $\tilde{z} = 0$. In particular, the numerical solutions were computed using the Mathematica² routine `NDsolve`.

For the sake of definiteness, we will now refer to the specific case of a galaxy with a gaseous disc and a stellar disc, thus we will use the equations of Section 3.1, replacing the subscript “1” with “gas” and the subscript “2” with “ \star ”. In this context, it is natural to assume that the effective gas pressure is $p_{\text{gas}} = \rho_{\text{gas}}\sigma_{\text{gas}}^2$, with $\sigma_{\text{gas}}^2 = k_{\text{B}}T/\bar{m} + \sigma_{\text{turb}}^2$, where T is the gas temperature, k_{B} is the

² Wolfram Research, Inc., Mathematica, Version 14.0, Champaign, IL (2024).

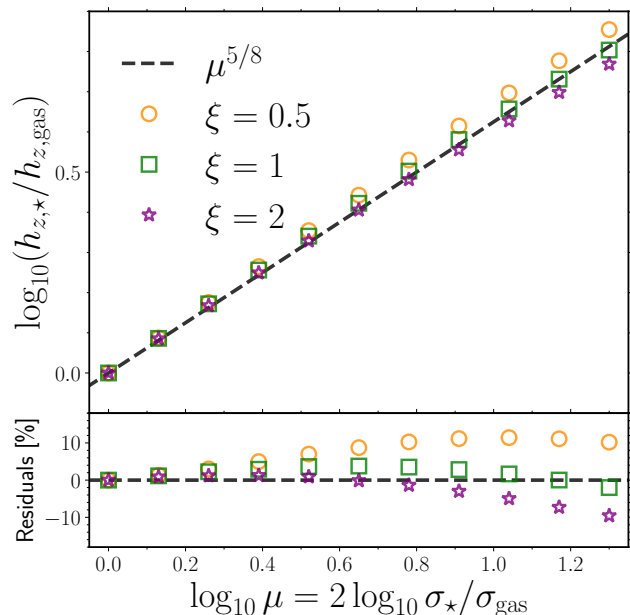


Fig. 2: Upper panel. Stars-to-gas thickness ratio $h_{z,\star}/h_{z,\text{gas}}$ as a function of the squared velocity-dispersion ratio μ for two-component isothermal slabs with different values of the midplane density ratio ξ ($h_z = h_{70\%}$, defined by Eq. 7). Overplotted in grey is the power law $\mu^{5/8}$. Lower panel. Per cent residuals between the points and the power law of the upper panel.

Boltzmann constant, \bar{m} is the mean molecular or atomic mass, and σ_{turb} is the turbulent velocity dispersion. This is motivated by the fact that there is observational evidence that galactic gaseous discs (either atomic or molecular) are turbulent and thus σ_{turb} contributes substantially to σ_{gas} (e.g. section 4.2.2 of Cimatti et al. 2019; Bacchini et al. 2020). Alternatively, the gas disc can be modelled as a discrete distribution of gas clouds (e.g. Jeffreson et al. 2022), in which case σ_{gas} is just the cloud-cloud velocity dispersion. The vertical structure of a stellar disc is described by the same equations used for a gas, but with σ_{\star} given by the vertical stellar velocity dispersion. Given that in a galaxy the stellar disc is in general dynamically hotter than the gaseous disc (at least for sufficiently old stellar populations; van der Kruit & Freeman 2011), without loss of generality, we will limit ourselves to explore cases with $\mu = \sigma_{\star}^2/\sigma_{\text{gas}}^2 \geq 1$.

An example of the numerically computed vertical density distributions of a two-component isothermal model with $\xi = 0.3$ and $\mu = 9$ is given in the upper panel of Fig. 1: for this model $\Sigma_{\star}/\Sigma_{\text{gas}} \approx 1.27$. For comparison, in the same diagram we also plot the vertical gas density distributions of a gaseous SGI slab with the same σ_{gas} and Σ_{gas} as the gaseous component of the two-component system and of a stellar SGI slab with the same σ_{\star} and Σ_{\star} as the stellar component of the two-component system. The stellar component, having higher velocity dispersion, is more vertically extended than the gaseous component. Comparing the solid and dashed curves in the upper panel of Fig. 1, it is apparent how, for given surface density and velocity dispersion, the volume density distribution depends on the presence or absence of a second component. Due to the deeper gravitational potential, in the presence of the stellar disc, the gaseous disc is more concentrated (i.e. with higher central volume density) than

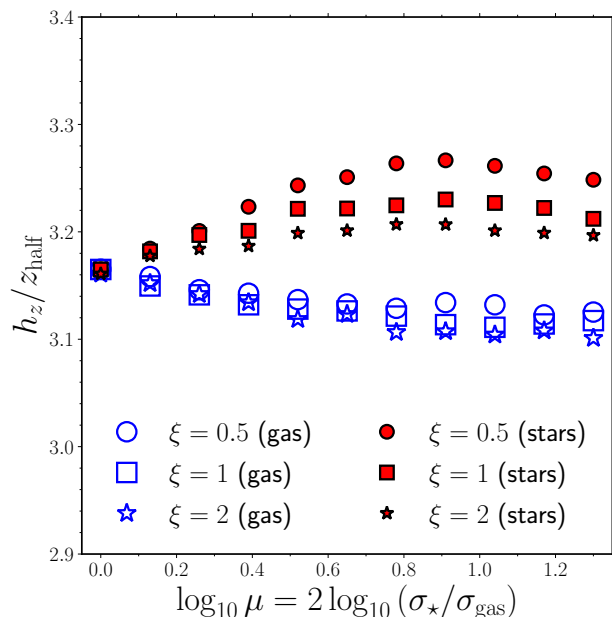


Fig. 3: Ratios $h_{z,\star}/z_{\text{half},\star}$ (filled symbols) and $h_{z,\text{gas}}/z_{\text{half},\text{gas}}$ (empty symbols) as functions of the squared velocity-dispersion ratio μ , for two-component isothermal slabs with different values of the midplane density ratio ξ . $h_z = h_{70\%}$ and z_{half} are defined by Eq. (7) and Eq. (2), respectively.

in the self-gravitating case, and, vice versa, in the presence of the gas disc, the stellar disc is more concentrated than in the self-gravitating case.

For given vertical gravitational field the scale height increases for increasing σ (see also Bacchini et al. 2019a). Computing numerically the ratios $z_{\text{half},\star}/z_{\text{half},\text{gas}}$ (see Eq. 2) and $h_{z,\star}/h_{z,\text{gas}}$ (see Eq. 7), we find that they are reasonably well described by the function $\mu^{5/8}$. This is illustrated in Fig. 2, where the ratio $h_{z,\star}/h_{z,\text{gas}}$ is compared with $\mu^{5/8}$ for $\xi = 0.5$, $\xi = 1$ and $\xi = 2$. A very similar behaviour is found for the scale-height ratio, if one defines the scale height of the i th component as $\Sigma_i/(2\rho_{0,i})$, as done in Romeo (1992, who find a slope 3/5) and Bertin & Pegoraro (2022, see their figure 2). Fig. 3 shows how the ratios $h_{z,\star}/z_{\text{half},\star}$ and $h_{z,\text{gas}}/z_{\text{half},\text{gas}}$ depend only weakly on μ and ξ in the explored range of values of these parameters. For μ close to unity, $h_{z,\star}/z_{\text{half},\star} \approx h_{z,\text{gas}}/z_{\text{half},\text{gas}} \approx 3.16$ independent of ξ . For large values of μ , $h_{z,\star}/z_{\text{half},\star} \approx 3.22$ and $h_{z,\text{gas}}/z_{\text{half},\text{gas}} \approx 3.12$, with a weak dependence on ξ .

3.3. Stability of each component assuming that the other component is unresponsive

We study here the local gravitational instability of the two-component discs introduced in Section 3.2, using the 3D instability criterion described in Section 2.1. This is possible for each of the two discs, under the simplifying assumption that the other disc is unresponsive, i.e. it acts just as fixed external gravitational potential and does not react dynamically to the perturbations (we discuss the effects of a responsive disc in Section 4). Though simplified, this approach is useful, because, given that the back reaction of the other component favours the instability (Toomre 1964), $Q_{3D} < 1$ is a sufficient condition for instability also in the presence of a responsive second component.

As in Section 3.2, we interpret one of the two components as a stellar disc. Stellar discs are collisionless system, so, strictly speaking, their gravitational stability or instability cannot be assessed with the same methods used for fluid systems. However, it has been shown that treating the stellar disc as a fluid is a good approximation, at least in 2D stability analyses (Bertin & Romeo 1988; Rafikov 2001; Romeo & Falstad 2013). To apply the criterion (5) to the stellar component, we thus assume that the stellar component has isotropic velocity dispersion tensor and we model it as a fluid (see Section 4.3 for a discussion). Here we assume that the gas and the stars undergo “isothermal” transformations, i.e. such that $d\rho_{\text{gas}} = \sigma_{\text{gas}}^2 d\rho_{\text{gas}}$ and $d\rho_{\star} = \sigma_{\star}^2 d\rho_{\star}$, which is in practice equivalent to use $\gamma = 1$ in the equations introduced in Section 2. In principle we could consider full axisymmetric disc models in which Σ_{gas} , σ_{gas} , κ and thus $Q_{\text{gas}} = \kappa\sigma_{\text{gas}}/(\pi G\Sigma_{\text{gas}})$, as well as the corresponding stellar quantities, vary as functions of R (see Bacchini et al. 2024). Instead, as done in section 5 of N23, we exploit the mapping between Q_{gas} and R to study the stability at given R , as a function of z , simply by fixing a value of Q_{gas} . Once Q_{gas} is fixed, Q_{\star} is determined by the condition $Q_{\star}/Q_{\text{gas}} = \sqrt{\mu}\Sigma_{\text{gas}}/\Sigma_{\star}$.

For the gaseous disc in the presence of stars, Q_{3D} can be computed numerically once $\rho_{\text{gas}}(z)$ and its derivative are computed, given that $p_{\text{gas}} = \sigma_{\text{gas}}^2 \rho_{\text{gas}}$ (with σ_{gas} independent of z) and that Q_{3D} (Eq. 5) can be rewritten for the gas component as

$$Q_{3D,\text{gas}}(z) = \frac{1}{\sqrt{2\tilde{\rho}_{\text{gas}}(z)}} \left[\sqrt{Q_{\text{gas}}^2 \tilde{\Sigma}_{\text{gas}}^2 + \frac{1}{\tilde{\rho}_{\text{gas}}^2(z)} \left(\frac{d\tilde{\rho}_{\text{gas}}}{dz} \right)^2} + \frac{1}{\tilde{h}_{z,\text{gas}}} \right] \quad (20)$$

Similarly, for the stellar component

$$Q_{3D,\star}(z) = \frac{1}{\sqrt{2\tilde{\rho}_{\star}(z)}} \left[\sqrt{\frac{Q_{\star}^2 \tilde{\Sigma}_{\star}^2}{\mu} + \frac{\mu}{\tilde{\rho}_{\star}^2(z)} \left(\frac{d\tilde{\rho}_{\star}}{dz} \right)^2} + \frac{\sqrt{\mu}}{\tilde{h}_{z,\star}} \right], \quad (21)$$

which can be obtained if $\rho_{\star}(z)$ and its derivative are known numerically. In the above equations, where we have used $\gamma = 1$, $\tilde{\rho}_{\text{gas}} = \rho_{\text{gas}}/\rho_{0,\text{gas}}$, $\tilde{\rho}_{\star} = \rho_{\star}/\rho_{0,\text{gas}}$, $\tilde{h}_{z,\text{gas}} = h_{z,\text{gas}}/b_{\text{gas}}$, $\tilde{h}_{z,\star} = h_{z,\star}/b_{\text{gas}}$, $\tilde{\Sigma}_{\text{gas}} \equiv \Sigma_{\text{gas}}/(2b_{\text{gas}}\rho_{0,\text{gas}})$ and $\tilde{\Sigma}_{\star} \equiv \Sigma_{\star}/(2b_{\text{gas}}\rho_{0,\text{gas}})$, where $b_{\text{gas}} \equiv \sigma_{\text{gas}}/\sqrt{2\pi G\rho_{0,\text{gas}}}$.

Profiles of Q_{3D} for the gaseous and stellar components are shown as solid curves in the lower panel of Fig. 1, assuming $Q_{\text{gas}} = 0.6$, for the same two-component disc models as in the upper panel of Fig. 1. For comparison, in the lower panel of Fig. 1 we plot as dashed curves Q_{3D} (Eq. 11) for the corresponding SGI gas and stellar discs with the same surface density, velocity dispersion and Q . This example illustrates that the presence of a second component can affect Q_{3D} in different ways: in this case, close to the midplane the gas disc has higher $Q_{3D,\text{gas}}$ in the presence than in the absence of the stellar disc (at fixed Q_{gas} , Σ_{gas} and σ_{gas}), while the stellar disc has lower $Q_{3D,\star}$ in the presence than in the absence of the stellar disc (at fixed Q_{\star} , Σ_{\star} and σ_{\star}). This occurs because Q_{3D} depends not only on the volume density (which, close to the midplane, is invariably higher in the presence of a second component, for given Σ and σ), but also on the shape of the vertical density profile, through $(d\rho_i/dz)/\rho_i$ and $h_{z,i}$ (see Eqs. 20 and 40).

A systematic study of the family of two-component isothermal disc models with $Q_{\text{gas}} = 0.6$ for a range of values of μ and ξ is displayed as an illustrative example in Fig. 4, which shows

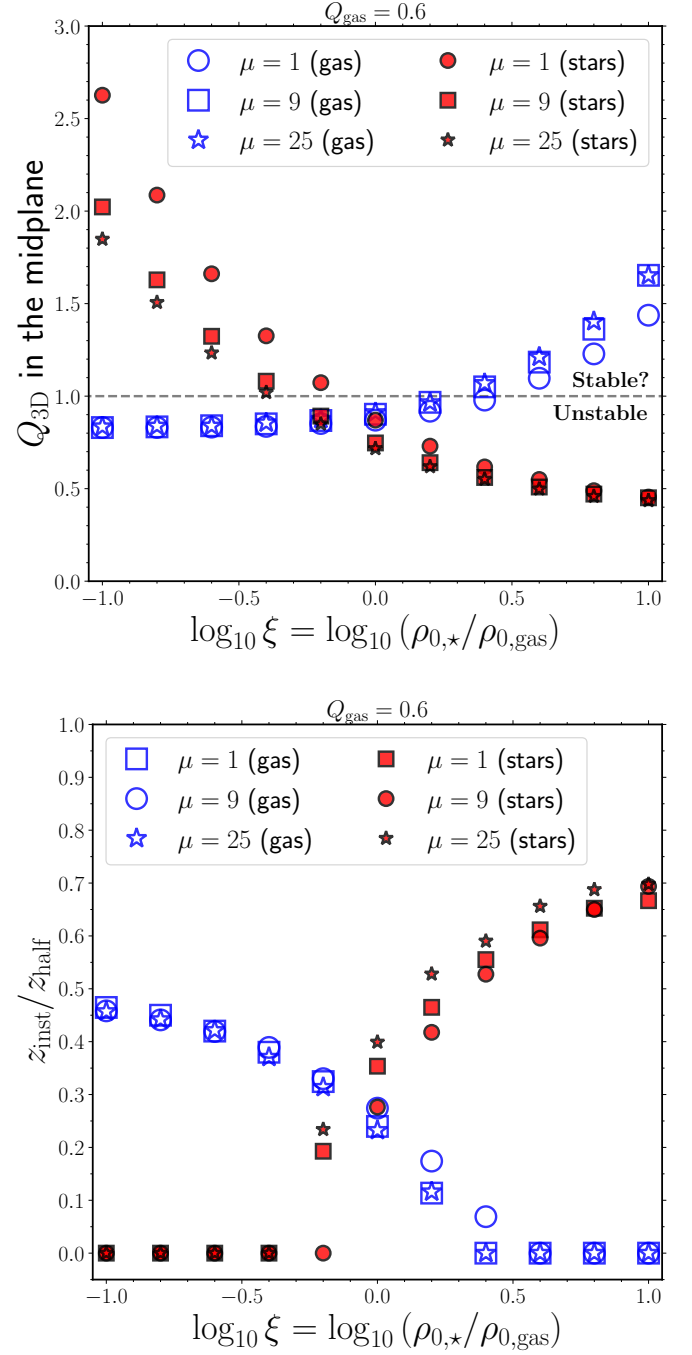


Fig. 4: Upper panel. Midplane values of $Q_{3D,\star}$ (filled symbols) and $Q_{3D,\text{gas}}$ (empty symbols) as functions of the midplane star-to-gas density ratio ξ , for different values of the star-to-gas squared velocity dispersion ratio μ . The horizontal dashed line indicates the instability threshold $Q_{3D} = 1$. Lower panel. Extent of the unstable strip above the midplane for the stellar ($z_{\text{inst},\star}$, normalized to $z_{\text{half},\star}$; filled symbols) and gaseous ($z_{\text{inst,gas}}$, normalized to $z_{\text{half,gas}}$; empty symbols) as functions of ξ for different values of μ . In both panels we assume $Q_{\text{gas}} = 0.6$.

that for the considered values of Q_{gas} there is always instability in the midplane, in the sense that either $Q_{3D,\text{gas}}(0) < 1$ or $Q_{3D,\star}(0) < 1$, and that the behaviour of the system depends weakly on μ . In particular, from the upper panel of Fig. 4, plot-

ting $Q_{3D,\text{gas}}(0)$ and $Q_{3D,\star}(0)$ as functions of ξ , we see that when the gas disc is dominant (low ξ) the instability is driven by the gas disc ($Q_{3D,\text{gas}}(0) < 1$), while when the stellar disc is dominant (high ξ) the instability is driven by the stars ($Q_{3D,\star}(0) < 1$). The lower panel of Fig. 4 shows, for each component in units of its z_{half} , the (above or below midplane) extent z_{inst} of the unstable region, defined by the condition $Q_{3D}(z) < 1$ for $z < z_{\text{inst}}$ and $Q_{3D}(z) > 1$ for $|z| > z_{\text{inst}}$. When one of the components is dominant ($\xi \ll 1$ or $\xi \gg 1$), we have $0.5 \lesssim z_{\text{inst}}/z_{\text{half}} \lesssim 0.7$ for $Q_{\text{gas}} = 0.6$. When the two components are comparable ($\xi \approx 1$) $z_{\text{inst}}/z_{\text{half}} \approx 0.3$ for $Q_{\text{gas}} = 0.6$. Fig. 4 suggests that the Q_{3D} -based stability properties of two-component discs are essentially independent of μ . At fixed Q_{gas} , the midplane density ratio ξ determines which component drives the instability, but influences only weakly the overall instability properties of the system: the minimum between $Q_{3D,\text{gas}}(0)$ and $Q_{3D,\star}(0)$ varies only by about a factor of two when ξ spans two orders of magnitude (see upper panel of Fig. 4). We recall, however, that the analysis based on Q_{3D} does not capture the full complexity of the problem of the instability of two-component discs, in which the coupling between stellar and gaseous perturbations plays an important role (e.g. Bertin & Romeo 1988; Romeo & Falstad 2013). The effect of this coupling in 3D two-component discs is discussed in the next section.

4. Stability of two-component discs when both components are responsive

In Section 3.3 we studied the stability a 3D gaseous disc in the presence of a stellar disc, but neglecting the back-reaction of the stellar disc, and vice versa. Here we attempt to address the more realistic, but more complicated question of the instability of a 3D two-component disc when both components are responsive. As done in Section 3.3, we assume for simplicity that both components can be treated as fluids (even in the case in which one of the components is a stellar disc). The limitations of this assumption are discussed in Section 4.3).

4.1. Linear perturbation analysis

The governing equations are, for each component, the same as in section 2.1 of N23, but with the gravitational potential Φ given by the sum of the gravitational potentials of the two components (Eq. 12):

$$\begin{aligned} \frac{\partial \rho_i}{\partial t} + \frac{1}{R} \frac{\partial (R \rho_i u_{R,i})}{\partial R} + \frac{\partial (\rho_i u_{z,i})}{\partial z} &= 0, \\ \frac{\partial u_{R,i}}{\partial t} + u_{R,i} \frac{\partial u_{R,i}}{\partial R} + u_{z,i} \frac{\partial u_{R,i}}{\partial z} - \frac{u_{\phi,i}^2}{R} &= -\frac{1}{\rho_i} \frac{\partial p_i}{\partial R} - \frac{\partial \Phi}{\partial R} - \frac{\partial \Phi_{\text{ext}}}{\partial R}, \\ \frac{\partial u_{\phi,i}}{\partial t} + u_{R,i} \frac{\partial u_{\phi,i}}{\partial R} + u_{z,i} \frac{\partial u_{\phi,i}}{\partial z} + \frac{u_{R,i} u_{\phi,i}}{R} &= 0, \\ \frac{\partial u_{z,i}}{\partial t} + u_{R,i} \frac{\partial u_{z,i}}{\partial R} + u_{z,i} \frac{\partial u_{z,i}}{\partial z} &= -\frac{1}{\rho_i} \frac{\partial p_i}{\partial z} - \frac{\partial \Phi}{\partial z} - \frac{\partial \Phi_{\text{ext}}}{\partial z}, \\ \frac{p_i}{\gamma - 1} \left(\frac{\partial}{\partial t} + \mathbf{u}_i \cdot \nabla \right) \ln(p_i \rho_i^{-\gamma}) &= 0, \\ \frac{1}{R} \frac{\partial}{\partial R} \left(R \frac{\partial \Phi_i}{\partial R} \right) + \frac{\partial^2 \Phi_i}{\partial z^2} &= 4\pi G \rho_i, \end{aligned} \quad (22)$$

with $i = 1, 2$, where $\mathbf{u}_i = (u_{R,i}, u_{\phi,i}, u_{z,i})$ is the velocity of the i th component, $\Phi = \Phi_1 + \Phi_2$ and Φ_{ext} is any additional

gravitational potential (for instance that of the dark-matter halo) assumed fixed³.

Here, for each component, we make the same assumptions described in Section 2.1. The unperturbed system is a stationary rotating ($u_{\phi,i} \neq 0$) solution of Eqs. (22) with no meridional motions ($u_{R,i} = u_{z,i} = 0$), locally negligible radial pressure and density gradients, and $u_{\phi,1} = u_{\phi,2} = \Omega R$, with $\Omega = \Omega(R)$. We note that the fact that the radial pressure gradient is negligible in the unperturbed disc (i.e. $|dp_i/dR|/\rho_i \ll \Omega^2 R$) implies that the epicyclic approximation condition $\sigma_i \ll \kappa R$ (e.g. Bertin 2014) is satisfied. This can be seen by considering the following ordering:

$$\frac{\sigma_i^2}{R} \sim \sigma_i^2 \left| \frac{d \ln p_i}{dR} \right| \sim \frac{1}{\rho_i} \left| \frac{dp_i}{dR} \right| \ll \Omega^2 R \sim \kappa^2 R, \quad (23)$$

where we have used $|d \ln p_i/dR| \sim 1/R$ and $\kappa \sim \Omega$.

As in N23, we perturb the system (22) writing a generic quantity $q = q(R, z, t)$ (such as ρ_i , p_i , Φ_i or any component of \mathbf{u}_i) as $q = q_{\text{unp}} + \delta q$, where the (time independent) quantity q_{unp} describes the stationary unperturbed fluid and the (time dependent) quantity δq describes the Eulerian perturbation. From now on, without risk of ambiguity, we will indicate any unperturbed quantity q_{unp} simply as q . Limiting ourselves to a linear stability analysis, we consider small ($|\delta q/q| \ll 1$) perturbations. Given that the radial perturbations tend to be more unstable than the vertical ones (Goldreich & Lynden-Bell 1965a, N23), we consider purely radial disturbances with spatial and temporal dependence $\delta q \propto \exp[i(k_R R - \omega t)]$, where ω is the frequency, and k_R is the radial component of the wavevector, which we assume to be such that $|k_R|R \gg 1$, as it is standard in the short-wavelength approximation. Moreover, given that in the one-component case Q_{3D} is lowest in the midplane, for simplicity we focus only on the midplane, where we can adopt⁴ $\rho'_{z,i} = 0$ and $p'_{z,i} = 0$. Under these assumptions, the linearized perturbed equations are

$$\begin{aligned} -i\omega \delta \rho_i + ik_R \rho_i \delta u_{R,i} &= 0, \\ -i\omega \delta u_{R,i} - 2\Omega \delta u_{\phi,i} &= -i \frac{k_R}{\rho_i} \delta p_i - ik_R \delta \Phi_1 - ik_R \delta \Phi_2, \\ -i\omega \delta u_{\phi,i} + \frac{d(\Omega R)}{dR} \delta u_{R,i} + \Omega \delta u_{R,i} &= 0, \\ -i\omega \delta u_{z,i} &= 0, \\ -i\omega \frac{\delta p_i}{\rho_i} + i\gamma \omega \frac{\delta \rho_i}{\rho_i} &= 0, \\ -\left(k_R^2 + h_z^{-2}\right) \delta \Phi_i &= 4\pi G \delta \rho_i, \end{aligned} \quad (24)$$

with $i = 1, 2$, where the last equation is the perturbed Poisson equation in the form of equation 14 of N23. As done in the previous sections, also here we assume $h_z = h_{70\%}$ (Eq. 7; see Appendix A and Section 2.1 for a discussion).

The system (24) leads to the biquadratic dispersion relation

$$\omega^4 - (\alpha_1 + \alpha_2)\omega^2 + \alpha_1\alpha_2 - \beta_1\beta_2 = 0, \quad (25)$$

where we have defined

$$\alpha_i \equiv B + s - A \frac{s}{s + E_1}, \quad (26)$$

³ The back-reaction of a dark-matter halo is supposed to be negligible, because within the disc its volume density is expected to be significantly lower than the baryonic volume density.

⁴ The order of the dispersion relation obtained from the linear-perturbation analysis is higher when $\rho'_{z,i} \neq 0$ and $p'_{z,i} \neq 0$.

$$\alpha_2 \equiv B + \mu s - \xi A \frac{\mu s}{\mu s + E_2}, \quad (27)$$

$$\beta_1 = A \frac{s}{s + E_1} \quad (28)$$

and

$$\beta_2 = \xi A \frac{\mu s}{\mu s + E_2}, \quad (29)$$

with $B \equiv \kappa^2$, $s \equiv \gamma \sigma_1^2 k_R^2$, $A \equiv 4\pi G \rho_1$, $E_1 \equiv \gamma \sigma_1^2 h_{z,1}^{-2}$, $E_2 \equiv \gamma \sigma_2^2 h_{z,2}^{-2}$, $\mu \equiv \sigma_2^2 / \sigma_1^2$ and $\xi = \rho_{0,2} / \rho_{0,1}$.

The dispersion relation (25) is formally identical to that found by [Jog & Solomon \(1984b\)](#) in their 2D analysis, but with different definitions and physical meaning of the coefficients, so our stability analysis essentially follows that of section II of [Jog & Solomon \(1984b\)](#), see also [Hoffmann & Romeo 2012](#) for further analysis of the same dispersion relation). Eq. (25) has roots

$$\omega_{\pm}^2 = \frac{1}{2} \left[(\alpha_1 + \alpha_2) \pm \sqrt{(\alpha_1 + \alpha_2)^2 - 4(\alpha_1 \alpha_2 - \beta_1 \beta_2)} \right]. \quad (30)$$

It is straightforward to show that the argument of the square root is always positive, so the solutions are always real. Given that $\omega_-^2 \leq \omega_+^2$, we can focus on the root ω_-^2 to study the stability. When either $\alpha_1 < 0$ or $\alpha_2 < 0$, $\omega_-^2 < 0$, thus we have instability. We note that the condition $\alpha_1 < 0$ is equivalent to

$$F_1(k_R) \equiv \frac{As}{(s+B)(s+E_1)} > 1, \quad (31)$$

which, following the analysis reported in appendix B3 of [N23](#), leads to the sufficient condition for instability

$$\frac{\sqrt{B} + \sqrt{E_1}}{\sqrt{A}} < 1, \quad (32)$$

which is just $Q_{3D,1} < 1$ in the special case $\rho'_{z,1} = 0$ considered in this section. It is straightforward to show that $\alpha_2 < 0$, i.e.

$$F_2(k_R) = \frac{\xi A \mu s}{(s+B)(\mu s + E_2)} > 1, \quad (33)$$

leads to

$$\frac{\sqrt{B} + \sqrt{E_2}}{\sqrt{A}} < 1, \quad (34)$$

that is $Q_{3D,2} < 1$ when $\rho'_{z,2} = 0$. Thus, as expected, when one of the components has $Q_{3D} < 1$ in the midplane (i.e. it would be unstable, neglecting the back-reaction of the other component), the two-component system results unstable also when the back-reaction is accounted for.

When both $\alpha_1 > 0$ (i.e. $F_1 < 1$) and $\alpha_2 > 0$ (i.e. $F_2 < 1$), the condition to have $\omega_-^2 < 0$ (and thus instability) is

$$\alpha_1 \alpha_2 - \beta_1 \beta_2 < 0, \quad (35)$$

i.e.

$$F_{1+2}(k_R) = F_1(k_R) + F_2(k_R) > 1, \quad (36)$$

where the destabilizing effect of the second responsive component is apparent. This is a manifestation of the fact that, because of the mutual back-reactions of the two components, a two-component system can be gravitationally unstable even when each component would be stable if taken individually.

When $Q_{3D,1} > 1$ and $Q_{3D,2} > 1$, and thus $F_1 < 1$ and $F_2 < 1$ for all k_R , $F_{1+2} > 1$ is a sufficient condition for instability.

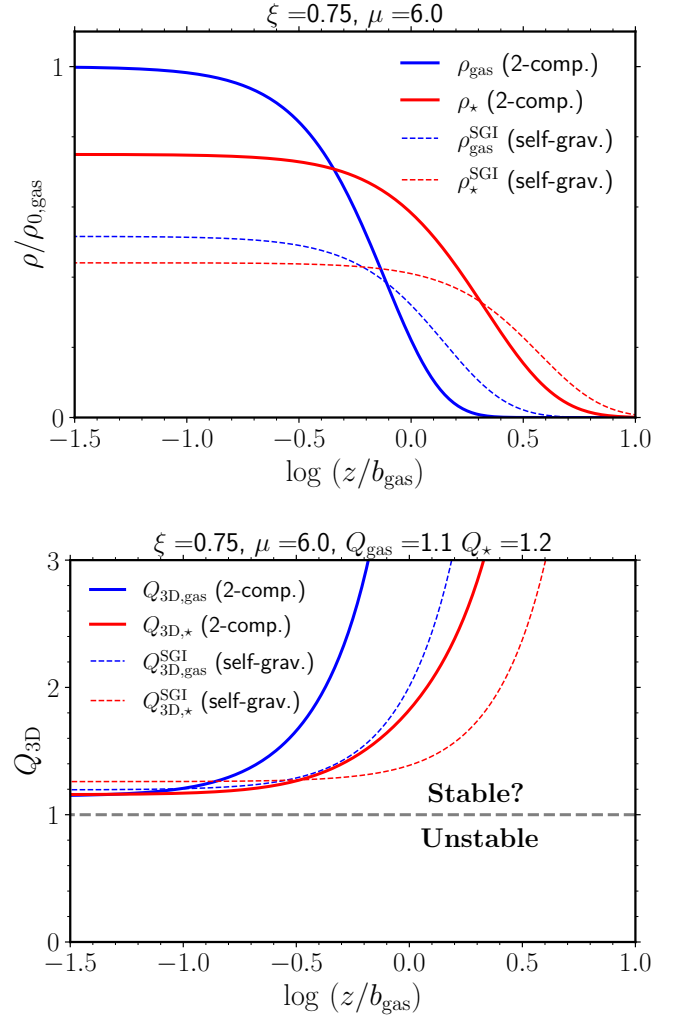


Fig. 5: Same as Fig. 1, but for a two-component isothermal disc model with $\xi = 0.75$, $\mu = 6$, $Q_{\text{gas}} = 1.1$ and $Q_{\star} = 1.2$.

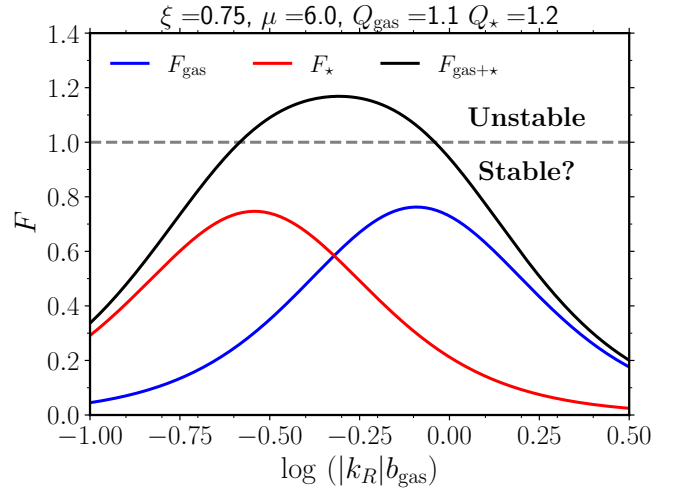


Fig. 6: The functions $F_{\text{gas}}(k_R)$, $F_{\star}(k_R)$ and $F_{\text{gas}+\star}(k_R)$ (see Eqs. 37, 38 and 39) for the same model as in Fig. 5. The unstable perturbations are those with $F_{\text{gas}+\star} > 1$.

4.2. Application to two-component discs with stellar and gaseous components

In order to apply quantitatively the results of Section 4.1, let us specialize to the case of a two-component disc with gas and stellar components. Relabeling now the component indices 1 and 2 as “gas” and “ \star ”, respectively, as done in Sections 3.2 and 3.3, it follows from the calculations of Section 4.1 that when either $Q_{3D,\text{gas}} < 1$ or $Q_{3D,\star} < 1$ in the midplane, we have instability. Let us thus focus on the case in which in the midplane $Q_{3D,\text{gas}} > 1$ and $Q_{3D,\star} > 1$, so that for all k_R we have $\alpha_{\text{gas}} > 0$ and $\alpha_\star > 0$, which, using the definitions (31) and (33) can be written, respectively, as

$$F_{\text{gas}}(k_R) = \frac{2\tilde{k}_R^2}{(\gamma\tilde{k}_R^2 + Q_{\text{gas}}^2\tilde{\Sigma}_{\text{gas}}^2)(\tilde{k}_R^2 + \tilde{h}_{z,\text{gas}}^{-2})} < 1 \quad (37)$$

and

$$F_\star(k_R) = \frac{2\xi\tilde{k}_R^2}{(\mu\gamma\tilde{k}_R^2 + Q_\star^2\tilde{\Sigma}_\star^2/\mu)(\tilde{k}_R^2 + \tilde{h}_{z,\star}^{-2})} < 1, \quad (38)$$

where $\tilde{k}_R \equiv k_R b_{\text{gas}}$. The condition for a disturbance with radial wavenumber k_R to be unstable is Eq. (36), which in this case reads

$$F_{\text{gas}+\star}(k_R) \equiv F_{\text{gas}}(k_R) + F_\star(k_R) > 1. \quad (39)$$

We then consider two-component isothermal discs in which the vertical distributions are computed numerically as described in Section 3.2. In the example shown in Figs 5 and 6, where we assume $\gamma = 1$ as done in Section 3.3, the values of the parameters ($\xi = 0.75$, $\mu = 8$, $Q_{\text{gas}} = 1.1$ and $Q_\star = 1.2$) are such that the two-component isothermal disc would not be considered unstable according to the analysis of Section 3.3, but turns out to be unstable when the back-reaction of one component onto the other is taken into account. Similar to the model shown in Fig. 1, the model shown in Fig. 5, for which $\Sigma_\star/\Sigma_{\text{gas}} \simeq 2.26$, has higher gas than stellar density close to the midplane (see upper panel of Fig. 5), but κ is assumed to be such that $Q_{3D,\text{gas}} > 1$ and $Q_{3D,\star} > 1$ (see lower panel of Fig. 5). Nevertheless, the system is gravitationally unstable, because there is a range of values of the wavenumber such that $F_{\text{gas}+\star} > 1$ (Fig. 6).

We stress that the criterion (39) can be applied to observed discs, because all the coefficients of the functions F_{gas} and F_\star can be estimated from observable quantities. In particular, to fully determine the function $F_{\text{gas}+\star}(k_R)$ at given R one needs estimates of Σ_{gas} , Σ_\star , $\rho_{0,\text{gas}}$, $\rho_{0,\star}$, $h_{z,\text{gas}}$, $h_{z,\star}$, σ_{gas} , σ_\star , and κ , which can all be inferred from observational data (see Bacchini et al. 2024). Then, to draw conclusions on the local gravitational instability of the system at given R in the disc midplane, it is sufficient to evaluate $F_{\text{gas}+\star}$ over a range of values of $|k_R|$, with lower limit between $1/R$ and $1/h_z$ (see Section 4.1) and upper limit $\gg 1/h_z$ (because the unstable disturbances have $|k_R|h_z$ of the order of unity; Goldreich & Lynden-Bell 1965a; N23).

4.3. Limitations of the application to stellar discs

In Sections 3.3, 4.1 and 4.2, we assumed that the component interpreted as a stellar disc has isotropic velocity dispersion tensor and we treated it as a fluid in the perturbation analysis. This approach has some limitations, which we discuss here. In the case of 2D disc models, comparisons between fluid and kinetic stability analyses (e.g. Rafikov 2001) have shown that modelling a stellar disc as a fluid turns out to be a sufficiently good approximation,

provided the quantity entering the disc gravitational instability diagnostics are correctly interpreted in terms of the collisionless quantities. For instance, it is the radial stellar velocity dispersion $\sigma_{\star,R}$ that enters the definition of Q_\star . Extending the same line of reasoning to our 3D analysis, when assuming that Q_{3D} is an approximate instability indicator for collisionless discs, we have to take care of relating the fluid quantities appearing in Q_{3D} to collisionless quantities. As it is clear from the analysis of N23 (see also Eqs. 22 and 24), the sound speed $c_s = \gamma\sigma$ appearing in Eq. (5) derives from a radial derivative of the pressure, so in this case σ must be identified with $\sigma_{\star,R}$. The quantity $c_s^2/\gamma = \sigma^2$ appearing in v^2 (see Eq. 6) derives from a vertical derivative of the pressure, so in this case σ must be identified with the vertical velocity dispersion $\sigma_{\star,z}$. Finally, the scale height h_z , for given midplane density, is expected to increase for increasing $\sigma_{\star,z}$, while being independent of $\sigma_{\star,R}$.

Focusing for simplicity on the midplane (where we expect $v \approx 0$) and assuming $\gamma = 1$, we can thus rewrite Q_{3D} (Eq. 5) for a stellar disc as

$$Q_{3D,\star} \approx \sqrt{\frac{\kappa^2}{4\pi G\rho_{0,\star}} + \frac{\sigma_{\star,R}}{\sigma_{\star,z}} \left(\frac{h_z}{\sigma_{\star,z}/\sqrt{4\pi G\rho_{0,\star}}} \right)^{-1}}. \quad (40)$$

Given that neither the first term in the r.h.s. nor the quantity in parentheses depend on the velocity ellipsoid, this equation shows that, for instance, a stellar disc with $\sigma_{\star,R} > \sigma_{\star,z}$ has in fact higher $Q_{3D,\star}$ (and thus is more stable) than estimated under the assumption of isotropic ($\sigma_{\star,R}/\sigma_{\star,z} = 1$) velocity distribution. Similar considerations apply to the instability indicators considered in Sections 4.1 and 4.2, given the relationship between $Q_{3D,\star}$ and F_\star .

There is observational evidence (Gerssen & Shapiro Griffin 2012; Marchuk & Sotnikova 2017; Pinna et al. 2018; Mackereth et al. 2019; Mogotsi & Romeo 2019) that in present-day stellar discs the velocity dispersion tensor is in general anisotropic, with typically $\sigma_{\star,R} > \sigma_{\star,z}$, a finding which is supported also by theoretical models (Rodionov & Sotnikova 2013; Walo-Martín et al. 2021). The velocity ellipsoid of stars in higher-redshift disc is hard to measure observationally, but it is reasonable to expect that higher-redshift discs are dynamically younger and thus more isotropic, having inherited the velocity distribution from the gas from which their stars have formed. This picture is supported by the finding that in the Milky Way the vertical scale height of the youngest stellar population is similar to that of the cold gas disc (e.g. Bacchini et al. 2019b).

5. One-component self-gravitating discs with polytropic vertical distributions

The vertical structure of discs is often modelled as isothermal, but in fact the velocity dispersion can in general have a vertical gradient. Here we explore how the stability properties of a stratified disc depend on such gradient, by exploring one-component self-gravitating discs with polytropic vertical distributions.

5.1. Equations

For a self-gravitating disc with polytropic vertical distribution, at given R

$$p(z) = p_0 \left[\frac{\rho(z)}{\rho_0} \right]^{\gamma'}, \quad (41)$$

where $\gamma' \equiv 1 + 1/n$ is the polytropic exponent, n is the polytropic index, $\rho_0 = \rho(0)$ and $p_0 = p(0)$. We assume that the gas is in vertical hydrostatic equilibrium in its own gravitational potential, so the vertical stratification is the same as that of a polytropic slab (chapter 2 of Horedt 2004; see also Ibanez & Sigalotti 1984). Eq. (41), combined with the hydrostatic equilibrium equation

$$\frac{dp}{dz} = -\rho \frac{d\Phi}{dz}, \quad (42)$$

and with the Poisson equation

$$\frac{d^2\Phi}{dz^2} = 4\pi G\rho, \quad (43)$$

gives for finite n the Lane-Emden equation

$$\frac{d^2\theta}{d\zeta^2} = \pm\theta^n, \quad (44)$$

where $\theta \equiv (\rho/\rho_0)^{1/n}$ and

$$\zeta \equiv z / [(n+1)p_0 / (4\pi G\rho_0^2)]^{1/2}. \quad (45)$$

In the right hand side of Eq. (44) the sign is minus when $-1 < n < \infty$ (i.e. $\gamma' < 0 \cup \gamma' > 1$), while it is plus when $-\infty < n < -1$ (i.e. $0 < \gamma' < 1$). When $n = \pm\infty$ ($\gamma' = 1$), combining Eqs. (41-43) we get

$$\frac{d^2\theta}{d\zeta^2} = e^{-\theta}, \quad (46)$$

whose analytic solution is the SGI slab described in Section 2.2. We assume that the fluid undergoes barotropic transformations of the form $p \propto \rho^\gamma$, so $dp = \gamma(p/\rho)d\rho$ and $c_s^2 = \gamma\sigma^2$. We limit ourselves to convectively stable polytropic distributions, i.e. satisfying the Schwarzschild stability criterion $\gamma' \leq \gamma$. In particular, in this section we consider two representative specific cases.

1. A monoatomic ideal gas undergoing adiabatic transformations with $\gamma = 5/3$, for which $c_s = \sqrt{5/3}\sigma$ and convectively stable distributions are those with $\gamma' \leq 5/3$, (i.e. $n < 0 \cup n \geq 3/2$).
2. A fluid undergoing isothermal transformations with $\gamma = 1$, for which $c_s = \sigma$ and convectively stable distributions are those with $\gamma' \leq 1$ ($n \leq 0$).

We note however that for $\gamma' < 0$ ($-1 < n < 0$) the density increases for increasing distance from the midplane (Viala & Horedt 1974), so in all cases we exclude from our analysis $\gamma' < 0$ ($-1 < n < 0$).

5.2. Vertical density and velocity-dispersion profiles

Given that we focus on the cases $\gamma = 5/3$ and $\gamma = 1$, and that we require convective stability (see Section 5.1), we present here polytropic distributions with polytropic exponent in the range $0 < \gamma' \leq 5/3$ (i.e. $n \geq 3/2 \cup n < -1$).

We solved numerically Eq. 44 with boundary conditions $\theta = 0$ and $d\theta/\partial\zeta = 0$ at $\zeta = 0$ using the Mathematica routine NDSolve. We find it convenient to normalize the vertical coordinate z to the half-mass half-height z_{half} . The vertical density and velocity-dispersion profiles are shown in Fig. 7. Note that the velocity dispersion σ is defined by $\sigma^2 = p/\rho$, so the profiles in the lower panel of Fig. 7 can also be interpreted as profiles of \sqrt{T} for a disc vertically supported by thermal pressure. We verified that the profiles shown in Fig. 7 are consistent with those tabulated by Ibanez & Sigalotti (1984) and Horedt (2004) for the values of n that we have in common.

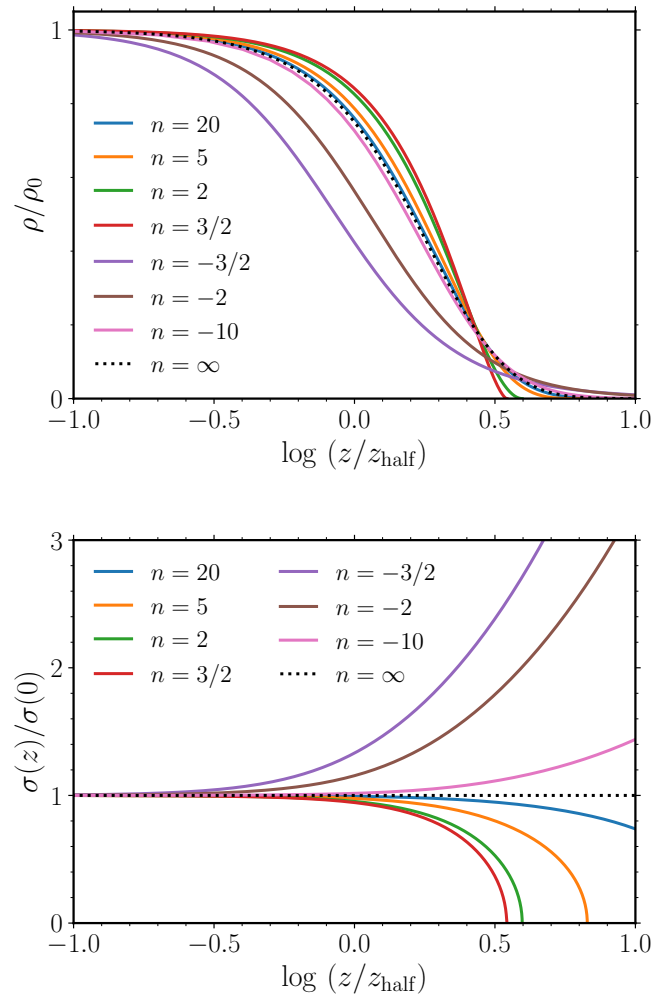


Fig. 7: Vertical density (upper panel) and velocity-dispersion (lower panel) profiles (solid curves) of one-component self-gravitating slabs with polytropic vertical distributions for different values of the polytropic index n . The case $n = \infty$ (dotted curves) is the analytic SGI vertical distribution.

5.3. Stability

We discuss here the stability of the self-gravitating discs based on the 3D instability criterion (Eq. 5). When $\gamma = 5/3$ we explore polytropic distributions with polytropic exponent in the range $0 < \gamma' \leq 5/3$ (i.e. $n \geq 3/2 \cup n < -1$). When $\gamma = 1$ we explore polytropic distributions with polytropic exponent in the range $0 < \gamma' \leq 1$ (i.e. $n < -1$). With these choices, the systems are guaranteed to be convectively stable. Fig. 8 shows vertical Q_{3D} profiles for models with $Q = 0.4$ for a selection of values of n for $\gamma = 5/3$ (upper panel) and $\gamma = 1$ (lower panel). The Q_{3D} profiles are qualitatively similar for all values of γ and n , with instability close to the midplane and Q_{3D} increasing with z . The instability strip $|z| < z_{\text{inst}}$ (see Section 3.3) tends to be slightly wider for higher n , though $z_{\text{inst}}/z_{\text{half}}$ spans a small range: $0.35 \lesssim z_{\text{inst}}/z_{\text{half}} \lesssim 0.54$ for $Q = 0.4$. The value $Q = 0.4$ adopted in Fig. 8 is such to have an unstable region around the midplane for all the explored values of n . The effect of increasing Q is to “shift upwards” the curves in Fig. 8, thus decreasing the extent

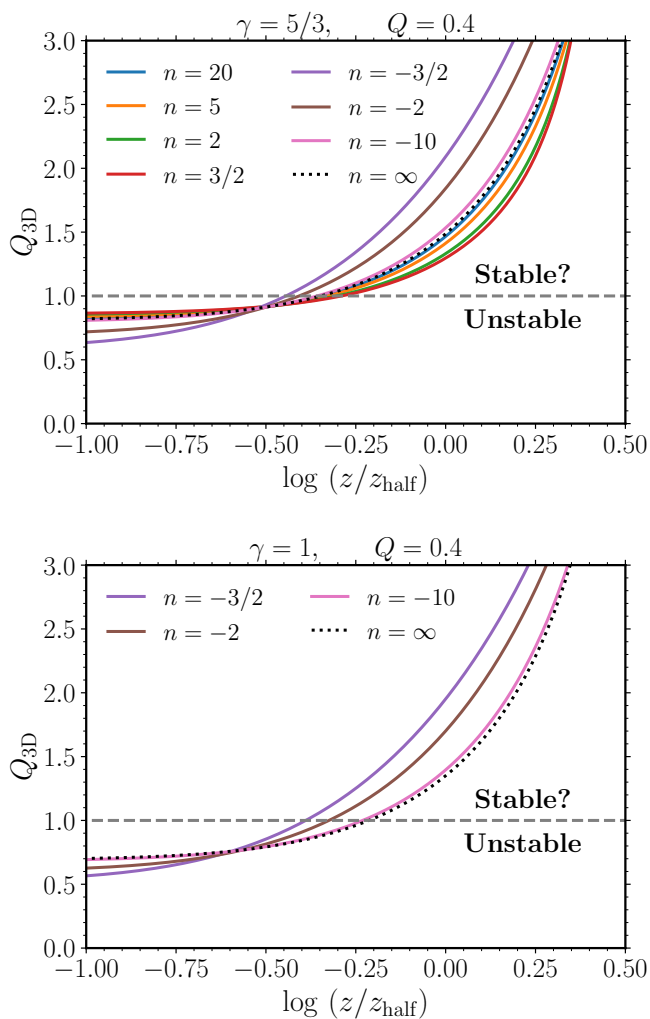


Fig. 8: Vertical profiles of the local gravitational instability parameter Q_{3D} for discs with polytropic vertical density distributions assuming $Q = 0.4$, when $\gamma = 5/3$ (upper panel) or $\gamma = 1$ (lower panel). In each panel the selected values of n are such that the distribution is convectively stable for the assumed γ . The case $n = \infty$ is the SGI, for which $Q_{3D}(z)$ is analytic. The horizontal dashed line indicates the instability threshold $Q_{3D} = 1$.

of the unstable regions, which gradually shrink to zero, starting from polytropic models with the lowest positive values of n .

6. Conclusions

Building on the 3D instability analysis of [Nipoti \(2023\)](#), we have studied the local gravitational instability in two-component 3D axisymmetric discs. We have focused on two-component isothermal discs (without vertical velocity dispersion gradients), but we have complemented our analysis with one-component self-gravitating polytropic discs (with vertical velocity dispersion gradients). The main results of this paper are the following.

- Given that the effect of a second responsive disc is to favour the instability, for each component of a two-component disc $Q_{3D} < 1$ is a sufficient condition for instability. Under the assumption that the vertical distributions are isothermal, Q_{3D} can be computed for each component at given radius R as a

function of distance from the midplane z using observational estimates of the surface densities, velocity dispersions and of the epicycle frequency κ .

- At given R and z , and at fixed surface density, velocity dispersion and κ (thus at fixed 2D Q parameter), the 3D Q_{3D} parameter of a disc can be higher, but can also be lower in the presence than in the absence of a second component (see lower panel of Fig. 1). When present, the instability occurs in a strip enclosing the midplane with half-height z_{inst} , which can be computed numerically from observationally inferred quantities.
- We derived a sufficient condition for local gravitational instability of two-component vertically stratified discs that takes into account the mutual back-reactions of the two discs. For instance, a disc consisting of a gaseous disc (index ‘gas’) and a stellar disc (index ‘ \star ’), with $Q_{3D,\text{gas}} > 1$ and $Q_{3D,\star} > 1$ at a given R , is unstable in the midplane against radial perturbations with wavenumber k_R , if $F_{\text{gas}+\star}(k_R) > 1$, where $F_{\text{gas}+\star}$ is a function that can be expressed in terms of observationally inferred quantities (see Section 4.2).
- We have computed $Q_{3D}(z)$, at given R , for one-component self-gravitating discs with vertical polytropic distributions and thus vertical temperature or velocity-dispersion gradients. For a range of values of the polytropic index n corresponding to convectively stable configurations, we found a behaviour qualitatively similar to discs with vertical isothermal distributions ($n = \infty$). For unstable models, the height of the instability region increases only slightly with n , at fixed Q .

In conclusion, the exploration of this paper provides support to the proposal that $Q_{3D} < 1$ is a robust sufficient condition for local gravitational instability of discs, which depends only weakly on the presence of a second component and on the vertical velocity-dispersion gradient. When $Q_{3D} > 1$, the local gravitational instability of a two-component disc can be tested by applying the wavenumber-dependent criterion (39). In conclusion, whenever the observational data allow to reconstruct the 3D properties of discs (see [Bacchini et al. 2024](#)), 3D local gravitational instability criteria such as those analyzed in this work can be successfully employed.

Acknowledgements

We thank the referee Alessandro Romeo for useful comments that helped improve the paper. The research activities described in this paper have been co-funded by the European Union – NextGenerationEU within PRIN 2022 project n.20229YBSAN - Globular clusters in cosmological simulations and in lensed fields: from their birth to the present epoch.

References

- Bacchini, C., Fraternali, F., Iorio, G., & Pezzulli, G. 2019a, *A&A*, 622, A64
Bacchini, C., Fraternali, F., Iorio, G., et al. 2020, *A&A*, 641, A70
Bacchini, C., Fraternali, F., Pezzulli, G., et al. 2019b, *A&A*, 632, A127
Bacchini, C., Nipoti, C., Iorio, G., et al. 2024, *A&A*, in press, arXiv:2405.00103
Behrendt, M., Burkert, A., & Schartmann, M. 2015, *MNRAS*, 448, 1007
Bertin, G. 2014, *Dynamics of Galaxies* (Cambridge University Press)
Bertin, G. & Amorisco, N. C. 2010, *A&A*, 512, A17
Bertin, G. & Casertano, S. 1982, *A&A*, 106, 274
Bertin, G. & Pegoraro, F. 2022, *European Physical Journal Plus*, 137, 538
Bertin, G. & Romeo, A. B. 1988, *A&A*, 195, 105
Chandrasekhar, S. 1961, *Hydrodynamic and hydromagnetic stability* (Clarendon Press: Oxford University Press)

- Cimatti, A., Fraternali, F., & Nipoti, C. 2019, *Introduction to galaxy formation and evolution: from primordial gas to present-day galaxies* (Cambridge University Press)
- Elmegreen, B. G. 1995, *MNRAS*, 275, 944
- Elmegreen, B. G. 2011, *ApJ*, 737, 10
- Genkin, I. L. & Safronov, V. S. 1975, *Soviet Ast.*, 19, 189
- Gerssen, J. & Shapiro Griffin, K. 2012, *MNRAS*, 423, 2726
- Goldreich, P. & Lynden-Bell, D. 1965a, *MNRAS*, 130, 97
- Goldreich, P. & Lynden-Bell, D. 1965b, *MNRAS*, 130, 125
- Griv, E. & Gedalin, M. 2012, *MNRAS*, 422, 600
- Hoffmann, V. & Romeo, A. B. 2012, *MNRAS*, 425, 1511
- Horedt, G. P. 2004, *Polytropes - Applications in Astrophysics and Related Fields*, Vol. 306
- Ibanez, S. M. H. & Sigalotti, L. D. G. 1984, *ApJ*, 285, 784
- Jefferson, S. M. R., Sun, J., & Wilson, C. D. 2022, *MNRAS*, 515, 1663
- Jog, C. J. & Solomon, P. M. 1984a, *ApJ*, 276, 127
- Jog, C. J. & Solomon, P. M. 1984b, *ApJ*, 276, 114
- Kato, S. 1972, *PASJ*, 24, 61
- Lin, C. C. & Shu, F. H. 1966, *Proceedings of the National Academy of Science*, 55, 229
- Mackereth, J. T., Bovy, J., Leung, H. W., et al. 2019, *MNRAS*, 489, 176
- Mackereth, J. T., Bovy, J., Schiavon, R. P., et al. 2017, *MNRAS*, 471, 3057
- Mamatsashvili, G. R. & Rice, W. K. M. 2010, *MNRAS*, 406, 2050
- Marchuk, A. A. & Sotnikova, N. Y. 2017, *MNRAS*, 465, 4956
- Meidt, S. E. 2022, *arXiv e-prints*, arXiv:2208.01888
- Mogotsi, K. M. & Romeo, A. B. 2019, *MNRAS*, 489, 3797
- Nipoti, C. 2023, *MNRAS*, 518, 5154
- O'Brien, J. C., Freeman, K. C., & van der Kruit, P. C. 2010, *A&A*, 515, A62
- Pinna, F., Falcón-Barroso, J., Martí, M., et al. 2018, *MNRAS*, 475, 2697
- Rafikov, R. R. 2001, *MNRAS*, 323, 445
- Rodionov, S. A. & Sotnikova, N. Y. 2013, *MNRAS*, 434, 2373
- Romeo, A. B. 1992, *MNRAS*, 256, 307
- Romeo, A. B. 1994, *A&A*, 286, 799
- Romeo, A. B. & Falstad, N. 2013, *MNRAS*, 433, 1389
- Romeo, A. B. & Wiegert, J. 2011, *MNRAS*, 416, 1191
- Safronov, V. S. 1960, *Annales d'Astrophysique*, 23, 979
- Shen, Y. & Lou, Y.-Q. 2003, *MNRAS*, 345, 1340
- Spitzer, Lyman, J. 1942, *ApJ*, 95, 329
- Toomre, A. 1964, *ApJ*, 139, 1217
- van der Kruit, P. C. & Freeman, K. C. 2011, *ARA&A*, 49, 301
- Vandervoort, P. O. 1970, *ApJ*, 161, 87
- Viala, Y. P. & Horedt, G. 1974, *A&A*, 33, 195
- Walo-Martín, D., Pérez, I., Grand, R. J. J., et al. 2021, *MNRAS*, 506, 1801
- Wang, B. & Silk, J. 1994, *ApJ*, 427, 759
- Wang, H.-H., Klessen, R. S., Dullemond, C. P., van den Bosch, F. C., & Fuchs, B. 2010, *MNRAS*, 407, 705
- Yim, K., Wong, T., Xue, R., et al. 2014, *AJ*, 148, 127

Appendix A: Gravitational potential of radial perturbations in thick discs

When studying radial axisymmetric linear perturbations in vertically stratified discs, N23, following Goldreich & Lynden-Bell (1965a), assumed a perturbed Poisson equation in the form

$$-\left(k_R^2 + h_z^{-2}\right) \delta\Phi = 4\pi G \delta\rho, \quad (\text{A.1})$$

which approximately accounts for the finite vertical extent of the disc. In Eq. (A.1), $\delta\Phi$ is the perturbed potential, $\delta\rho$ is the perturbed density, k_R is the perturbation wavenumber and h_z is the disc thickness. Following N23, we assume $h_z = h_{70\%}$ (Eq. 7), so the above equation becomes

$$-\left(k_R^2 + h_{70\%}^{-2}\right) \delta\Phi = 4\pi G \delta\rho. \quad (\text{A.2})$$

In this appendix we assess quantitatively the validity of this approximation of the perturbed Poisson equation. Let us consider an axisymmetric gravitational potential perturbation, which in cylindrical coordinates has the form

$$\delta\hat{\Phi}(R, z, t) = f(z) \exp[i(k_R R - \omega t)] \delta\hat{\Phi}_0, \quad (\text{A.3})$$

with $f(z)$ such that $f(0) = 1$, $\lim_{|z| \rightarrow \infty} f(z) = 0$ and $\delta\hat{\Phi}_0 = \delta\hat{\Phi}(0, 0, 0)$ constant, and a density perturbation in the form

$$\delta\hat{\rho}(R, z, t) = g(z) \exp[i(k_R R - \omega t)] \delta\hat{\rho}_0, \quad (\text{A.4})$$

with $g(z)$ such that $g(0) = 1$, $\lim_{|z| \rightarrow \infty} g(z) = 0$ and $\delta\hat{\rho}_0 = \delta\rho(0, 0, 0)$ constant. From the perturbed Poisson equation

$$\nabla^2 \delta\hat{\Phi} = 4\pi G \delta\hat{\rho}, \quad (\text{A.5})$$

assuming (as in the analysis of N23) that $1/R$ is negligible compared to $|k_R|$, we get

$$\frac{1}{A_0} \left(-k_R^2 f + \frac{d^2 f}{dz^2} \right) \exp[i(k_R R - \omega t)] \delta\hat{\Phi}_0 = \frac{4\pi G}{A_0} g(z) \exp[i(k_R R - \omega t)] \delta\hat{\rho}_0, \quad (\text{A.6})$$

which is satisfied for

$$g(z) = \frac{1}{A_0} \left(-k_R^2 f + \frac{d^2 f}{dz^2} \right) \quad (\text{A.7})$$

and

$$\delta\hat{\Phi}_0 = \frac{4\pi G}{A_0} \delta\hat{\rho}_0, \quad (\text{A.8})$$

where

$$A_0 \equiv -k_R^2 + \left(\frac{d^2 f}{dz^2} \right)_{z=0} \quad (\text{A.9})$$

is a normalization factor that ensures $g(0) = 1$. Indicating with $\langle \dots \rangle$ a weighted average in z , in our perturbed hydrodynamics equations we can approximate $\delta\hat{\Phi}$ with

$$\delta\Phi(R, t) \equiv \langle \delta\hat{\Phi} \rangle = \langle f \rangle \exp[i(k_R R - \omega t)] \delta\hat{\Phi}_0. \quad (\text{A.10})$$

Similarly, we can approximate $\delta\hat{\rho}(R, z, t)$ with

$$\delta\rho(R, t) \equiv \langle \delta\hat{\rho} \rangle = \langle g \rangle \exp[i(k_R R - \omega t)] \delta\hat{\rho}_0, \quad (\text{A.11})$$

where (see Eq. A.7)

$$\langle g \rangle = \frac{1}{A_0} \left(-k_R^2 \langle f \rangle + \left\langle \frac{d^2 f}{dz^2} \right\rangle \right). \quad (\text{A.12})$$

Let us specialize to the case in which

$$f(z) = e^{-\frac{z^2}{2H^2}} \quad (\text{A.13})$$

and adopt as weighted average of a generic function $F(z)$

$$\langle F(z) \rangle = \frac{\int_{-\infty}^{\infty} F(z) f(z) dz}{\int_{-\infty}^{\infty} f(z) dz}. \quad (\text{A.14})$$

For f given by Eq. (A.13) $A_0 = -(k_R^2 + H^{-2})$ (Eq. A.9), so, combining Eq. (A.7) and Eq. (A.13), we get

$$g(z) = \frac{k_R^2 + H^{-2} - z^2 H^{-4}}{k_R^2 + H^{-2}} e^{-\frac{z^2}{2H^2}}. \quad (\text{A.15})$$

Calculating explicitly the weighted averages over z , we get

$$\langle f \rangle = \int f^2(z) dz \Big/ \int f(z) dz = \frac{1}{\sqrt{2}} \quad (\text{A.16})$$

and

$$\langle g \rangle = \int g(z) f(z) dz \Big/ \int f(z) dz = \frac{1}{\sqrt{2}(k_R^2 + H^{-2})} \left(k_R^2 + \frac{1}{2H^2} \right). \quad (\text{A.17})$$

It follows that

$$\delta\Phi = \frac{1}{\sqrt{2}} \exp[i(k_R R - \omega t)] \delta\hat{\Phi}_0 \quad (\text{A.18})$$

and

$$\delta\rho = \frac{k_R^2 + \frac{1}{2}H^{-2}}{\sqrt{2}(k_R^2 + H^{-2})} \exp[i(k_R R - \omega t)] \delta\hat{\rho}_0. \quad (\text{A.19})$$

Combining the two above equations we get

$$\delta\rho = -\frac{k_R^2 + \frac{1}{2}H^{-2}}{k_R^2 + H^{-2}} \frac{\delta\hat{\rho}_0}{\delta\hat{\Phi}_0} \delta\Phi, \quad (\text{A.20})$$

which, using Eq. (A.8), gives

$$-\left(k_R^2 + \frac{1}{2}H^{-2}\right) \delta\Phi = 4\pi G \delta\rho. \quad (\text{A.21})$$

The above equation coincides with Eq. (A.2) if we assume

$$2H^2 = h_{70\%}^2. \quad (\text{A.22})$$

We conclude that, approximating the gravitational potential of the perturbation with its vertical weighted average, the perturbed Poisson equation in the form (A.2) is valid for a density perturbations with vertical profile

$$\frac{\delta\hat{\rho}(R, z, t)}{\delta\hat{\rho}(R, 0, t)} = g(z) = \frac{k_R^2 + H^{-2} - z^2 H^{-4}}{k_R^2 + H^{-2}} e^{-\frac{z^2}{2H^2}}, \quad (\text{A.23})$$

with $H^2 = h_{70\%}^2/2$.

We now want to verify whether assuming a perturbation with this vertical structure is consistent with the vertical structure of the unperturbed system. Let us consider for instance an unperturbed SGI vertical density profile (8): in this case $h_{70\%} \simeq 1.7346b$, so the assumption (A.22) becomes

$$H = \frac{1.7346}{\sqrt{2}} b = 1.2265b. \quad (\text{A.24})$$

Assuming $H^2 = h_{70\%}^2/2$, in the left-hand panel of Fig. A.1 we compare, for different values of $k_R H$, the normalized vertical density profile of the perturbation $\delta\hat{\rho}(R, z, t)/\delta\hat{\rho}(R, 0, t) = g(z)$ (with g given by Eq. A.15) with the normalized unperturbed vertical density profile $\rho(z)/\rho(0)$. The fact that the shape of the density profile of the perturbation is similar to that of the unperturbed density distribution suggests that the considered disturbance can be consistent with the hypothesis of small perturbations $|\delta\rho|/\rho \ll 1$. This is illustrated in the right-hand panel of Fig. A.1, showing the ratio $|\delta\hat{\rho}|/\rho$ as a function of z assuming, for instance, $\delta\hat{\rho}/\rho = 0.01$ in the midplane. We note that in Fig. A.1 the plotted range in z is such that it contains 90% of the mass per unit surface of the unperturbed distribution.

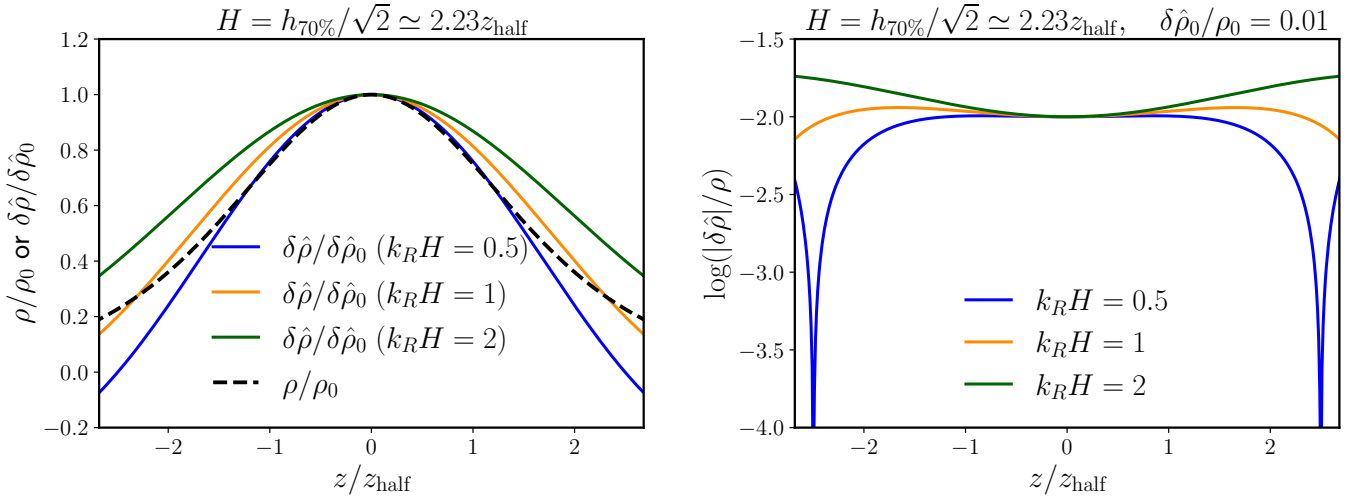


Fig. A.1: Left panel. Normalized vertical profiles of the density perturbation $\delta\hat{\rho}$ (Eqs. A.4 and A.15) with $H = h_{70\%}/\sqrt{2}$ for different values of the radial wavenumber k_R (solid curves), compared with the normalized unperturbed vertical density profile (Eq. 8; dashed curve). Right panel: vertical profiles of the ratio between the density perturbation and the unperturbed density profile for the same values of k_R as in the left panel, assuming $\delta\hat{\rho}/\rho = 0.01$ at $z = 0$. The plotted range in z encloses 90% of the mass per unit surface of the unperturbed distribution.